12,05

Functionalization of $Co_{1-x}Zn_xFe_2O_4$ nanoparticles with polyethylene glycol ($Co_{1-x}Zn_xFe_2O_4$@PEG) (at $x = 0$, 0.1, 0.2, 0.4 and 0.6) for biomedical applications

© A.S. Kamzin[1], V.G. Semenov[2], L.S. Kamzina[1]

[1] Ioffe Institute,
St. Petersburg, Russia
[2] St. Petersburg State University,
St. Petersburg, Russia

E-mail: ASKAM@mail.ioffe.ru

Received February 1, 2024
Revised February 1, 2024
Accepted February 2, 2024

Extensive research on magnetic nanoparticles (MNPs) has shown their enormous potential for use in various fields, including biomedicine. However, the created MNPs must have long-term colloidal stability, which is not an easy task, since chemical, physical, biological factors and conditions must be taken into account when synthesizing and functionalizing MNPs for a specific application. By regulating the nature of the core (particle), shell (coating) and ligands (coating material), it is possible to create nanocomposites (MNCs) with MNPs-term colloidal stability for a wide range of applications, including for the diagnosis and therapy of various diseases with the required biocompatibility and functionality. In this regard, the work is devoted to the synthesis of MNP $Co_{1-x}Zn_xFe_2O_4$, the functionalization (coating) of particles with polyethylene glycol (PEG) and studies of the effect of coating on the properties of the obtained MNCs $Co_{1-x}Zn_xFe_2O_4$@PEG. Fourier transform infrared spectroscopy (IR-PF), X-ray diffraction (XRD) and Mossbauer spectroscopy (MSp) were used to study the properties of MNPs and MNCs. The formation of a PEG layer on particles has been confirmed by infrared spectroscopy. The analysis of the Mossbauer spectra and distribution functions of effective magnetic fields suggests that during the functionalization of MNPs $Co_{1-x}Zn_xFe_2O_4$ particles with approximately the same properties combine and form clusters coated with a surfactant. Heating of MNC $Co_{1-x}Zn_xFe_2O_4$@PEG ($0 \le x \le 0.4$) the temperature required for hyperthermic therapy (44−46°C) is reached in 60 seconds when an external alternating magnetic field with a frequency of 2.0 MHz and a strength of 4.5 kA/m is applied. Synthesized and PEG-coated MNCs $Co_{1-x}Zn_xFe_2O_4$@PEG can be used for magnetic resonance imaging,

Keywords: agnetic nanoparticles, particle functionalization, magnetic liquids, Mossbauer spectroscopy.

DOI: 10.61011/PSS.2024.03.57949.15

1. Introduction

Combination of nanoscale dimensionality and uniqueness of the magnetic properties of the particles has resulted their use in diverse fields [1], including in biomedicine: cell separation, magnetic resonance imaging, medicine delivery and intracellular magnetic hyperthermia [2,3]. The use of magnetic nanoparticles (MNPs) in hyperthermia therapy and medicine delivery is motivated by MNP deliverability into a malignant tumor and heat generability of the magnetic particles into the tumor directly and their destructibility for tumor cells without health impact [2–5]. It is important that in case of using the MNPs having the Curie temperature within the range 42−48°C [3–5] the heating temperature is automatically limited and necrosis of healthy cells is eliminated.

The biomedicine nanotechnologies use the MNPs of hematite (α-Fe_2O_3), magnetite (Fe_3O_4) and maghemite (γ-Fe_3O_4), which are known due to their non-toxicity and high biocompatibility [4]. However, the magnetic characteristics and aggregability of these oxides in biomedicine suspensions do not meet biomedical requirements. It has stimulated studies of new MNPs of spinel ferrites MFe_2O_4 (M = Fe, Co, Zn, Ni, Mn), which are synthesized based on magnetite (Fe_3O_4). The biggest attention was paid to the MNPs of the ferrites $CoFe_2O_4$ and $ZnFe_2O_4$, which have different structure and degree of toxicity [6,7]. However, the biomedical application of the MNPs $CoFe_2O_4$ are limited by its toxicity. Zinc ferrite ($ZnFe_2O_4$) below the magnetic ordering temperature (9.5 K) has a normal spinel structure, wherein all the ions Zn^{2+} occupy the tetrahedral position, so do all the ions Fe^{8+} — the octahedral positions [1,6–9].

Search for the biocompatible MNPs with higher magnetic characteristics has resulted in double substitution ferrites $Tr_{1-x}M_xFe_2O_4$, wherein the Tr ions replaced the ions of two-valence metals (M), thereby substantially changing the structure of the initial ferrites [10–13]. The substitution of the cobalt ions in $CoFe_2O_4$ with the diamagnetic ions Zn^{2+} not only reduces toxicity [10], but improves parameters of the MNPs $Co_{1-x}Zn_xFe_2O_4$ (hereinafter referred to as CZFO) for the biomedical applications [11,12,14–16]. Introduction of the Zn ions in an amount from 5 to 15%

(in relation to Co) improves the hyperthermia efficiency of the MNPs CZFO, but further increase in the number of Zn^{2+} leads to the opposite effect [15]. Despite substantial achievements in MNP creation for biomedicine, they can be toxic, chemically unstable in a biological medium, etc. For this reason, it has suggested biocompatible ferrofluids (or magnetic liquids — ML) [17]. The magnetic liquids are high-stable colloidal suspensions of stabilized magnetic nanoparticles, which have simultaneously fluid and magnetic properties that are controlled and adjusted by means of magnets. In order to achieve the high colloidal stability of ML, the MNP surface is modified (functionalized) — it is covered such polymers as dextran, poly(vinyl alcohol), poly 3-caprolactone, polyvinyl-pyrrolidone, polyethylene glycol (PEG) (see [17–20] and references therein). Such MNP coatings are designed to ensure the change of the surface energy and reduction of particle aggregation. One of the most attractive polymers is polyethylene glycol (PEG), since it is soluble in both polar solvents and some non-polar solvents, hydrophilic, biocompatible, non-antigenic, protein-resistant [17–20], and it opens the way for being attached to drug MNPs [21].

The MNP properties are studied by means of diverse procedures, such as X-ray diffraction, energy-dispersive X-ray analysis, high-resolution transmission electron microscopy, vibrating-sample magnetometers (VSM), superconducting quantum interference magnetometers (SQUID), etc. [3,17]. The ferrites have various configurations of ferrum ions (Fe^{2+} and Fe^{3+}), octahedral or tetrahedral, surface and bulk positions, etc. Analysis of spectral components of the Mössbauer spectra (MS) makes it possible to identify these configurations and extract information on a phase composition, kinetics of a phase transition and properties of the magnetic materials with accuracy, which often exceeds capabilities of the know procedures [1,10,11,17].

Thus, by means of MS, it has been established that clusters were formed in superparamagnetic properties of the ferrum oxides covered by poly L,L-lactic or poly-ε-caprolactone acid, thereby resulting in enhancement of interactions between the particles [22]. The study [23] has synthesized Co ferrite MNPs by modifying a magnetite surface with cobalt nitrate, and with subsequent functionalization of the obtained particles $CoFe_2O_4$ with polyethyleneimine (PEI). The Mössbauer and X-ray studies have shown that stabilization of the particles $CoFe_2O_4$@PEI resulted in formation of additional phases α-Fe_2O_3, ε-Fe_2O_3 [22]. The studies of the MNPs of the ferrite $CoFe_2O_4$ (which were uncoated and coated by polypyrrole) [23] have shown that functionalization resulted in reduction of particle saturation magnetization, increase in the number of particles in a paramagnetic state and reduction of effective magnetic fields. The study [24] has shown that a magnetic structure of the surface layer of the MNPs of the magnetite depended on the nature of a functionalization material. Coating the MNPs with carboxylate causes a canted state of the surface layer of the particles, reducing particle saturation magnetization. Posphonated molecules coating the particles are joined by covalent bonds with the surface layer of the particles and the canted magnetic structure in the surface layer is not formed and saturation magnetization is not reduced [24]. The study [25] has established that a chitosan coating of the MNPs $MnFe_2O_4$ and $Mn_{0.5}Co_{0.5}Fe_2O_4$ increases the particle size and decreases lattice constants. Spontaneous magnetization of the chitosan-coated particles $MnFe_2O_4$ is reduced from 49.2 emu/g to 23.6 emu/g, so that of $Mn_{0.5}Co_{0.5}Fe_2O_4$ is from 63.2 emu/g to 33.2 emu/g, but it is still higher that of $MnFe_2O_4$. The chitosan-coated samples exhibit features of superparamagnetism and migration of the Fe ions between the octahedral and octahedral positions [25]. The studies of FFs consisting in the water-dispersed MNPs $CoFe_2O_4$ and Fe_3O_4, which are coated by two SAW layers, have shown various relaxation processes due to influence of the coating layers [26]. The study [27] has found a magnetic-dead layer of the thickness of 1 nm on the MNP surface, whose thickness substantially depends on a ferrite type, but does not depend on the coating type. The HFI parameters (a hyperfine field, quadrupole splitting and a line width) have substantially changed after functionalization of the ferrite particles, which was related to spin behavior in the MNP surface layer [28,29]. Based on the temperature MS studies of the phosphate-functionalized particles α-Fe_2O_3 of the size of 8 nm, it has been concluded that these particles have fast superparamagnetic relaxation that was suppressed in these particles when uncoated [30]. The MSes of the particles α-Fe_2O_3 of the size of 8 nm, coated and uncoated [31] have shown that a slope of the dependence H_{eff} on the temperature of the uncoated (therefore, mutually interacting) particles was less than for the coated (non interacting) MNPs [30].

Thus, there is a big number of the papers for studying impact of the coating on the MNP properties. However, it still requires the studies for investigating the properties of the functionalized MNPs in direct comparison with those observed in the uncoated particles, thereby significantly expanding understanding the impact of modification (coating). In this regard, the present study provides the results of investigating surface functionalizability of the MNPs $Co_{1-x}Zn_xFe_2O_4$ (hereinafter referred to as CZFO) with polyethylene glycol (PEG) and impact of this coating on the properties and colloidal stability of the magnetic nanocomposites (MNC) CZFO@PEG.

2. Materials and synthesis of the samples

2.1. Synthesis of MNPs $Co_{1-x}Zn_xFe_2O_4$ at $x = 0.0$, 0.1, 0.2, 0.4 and 0.6

The MNPs of the ferrites MFe_2O_4 are synthesized using various methods, namely, by solid-state reaction, combustion, sol-gel, auto-burning, microwave synthesis, hydrothermal method and that of codeposition [1–3,6–19,32]. In the last case, the nanoparticles are formed at lower

temperatures and often without high-temperature calcination. It is important that a synthesis technique determines the MNP size, distribution of the cations across the non-equivalent positions, the number of defects in the samples, i. e. the parameters that specify the properties and magnetic behavior of the ferrites. So, the synthesis technique is a key issue for producing the required ferrite.

The codeposition method is most often used for synthesizing MNPs of the average diameter below 50 nm. It has a number of advantages: low-cost and environment-friendly reagents are used instead of hazardous organic solvents; short time of the reaction; high crystallinity of the particles; no special flushing procedures are required [10–19]. That is why the MNPs of the spinel ferrite $Co_{1-x}Zn_xFe_2O_4$ (where $x = 0.0, 0.1, 0.2, 0.4$ and 0.6) have been synthesized by the method of chemical codeposition, which was modified in [10] and used in [11,12].

The nanoparticles CZFO have been synthesized by using $FeCl_3 \cdot 6H_2O$ (97%), $CoCl_2 \cdot 6H_2O$ (97%), $ZnCl_2$ (99%), sodium hydroxide (NaOH). All the materials were chemically pure reagents without additional purification. For synthesis of each composition, required amounts of $FeCl_3 \cdot 6H_2O$, $CoCl_2 \cdot 6H_2O$, $ZnCl_2$ for producing the stoichiometric compounds $Co_{1-x}Zn_xFe_2O_4$ were separately solved in double-distilled water (DDW). These cation solutions were thoroughly and intensely stirred in order to improve homogeneity. The heated NaOH (2 M) was dropped into the above-said solution for 1 h until it had been codeposited, and the pH value was 10. Then, the solution was held at 800°C for 1 h. This time was enough for forming hydroxides in the spinel ferrite. The precipitate was flushed in magnetic decantation with DDW. The product was dried in an electric oven at the temperature of 600°C overnight. Then, the dried powder was ground in an agate mortar to produce very fine particles and baked at 300°C for 3 h.

2.2. Functionalization of these particles $Co_{1-x}Zn_xFe_2O_4$ with polyethylene glycol (PEG)

In order to produce the water-dispersed and biocompatible magnetic nanocomposites $Co_{1-x}Zn_xFe_2O_4$@PEG (hereinafter referred to as CZFO@PEG), the nanoparticles CZFO were coated with polyethylene glycol (PEG). For this, the MNPs CZFO in the amount of 100 mg for 30 min under ultrasound treatment (400 W, 20 kGz) were dispersed in 50 mL into double distilled water. The PEG solution in the amount of 10 mL with the concentration of 2.5 mg/mL was poured slowly (but with vigorous mechanical stirring) into the produced suspension and then this mixture was held at 100°C for 2 h for quite good interaction of the PEG polymer and the MNPs CZFO. This procedure decreases MNP agglomeration as well as increases stability of dispersion of the CZFO particles in the polar medium. For 10 min this solution was processed with ultrasound and then held for 24 h and centrifugated at the speed of 8000 revs/min in order to remove the MNPs uncoated with the PEG molecules. The produced composites were flushed with DD water, ethanol and acetone in order to remove excessive unreacted chemical substances. After purification, the MNPs were dried in an ambient atmosphere.

3. Characterization of the synthesized particles

3.1. Experimental procedures

The phase purity and crystallinity of the synthesized particles CZFO and CZFO@PEG have been determined by means of X-ray diffractometry (XD) and Mössbauer spectroscopy (MS). The XPs were obtained within the range 2Θ from 20 to 80° using the Rigaku powder X-ray diffractometer with CuK_α-radiation at the wavelength of 0.1542 A within the range from 20 to 80°. The crystallite sizes were calculated by a Scherrer method [32].

The interaction of PEG with the MNPs was studied using the IR-Fourier-spectrometer VERTEX 70 within the frequency range from 4000 to 500 cm^{-1} with the attachment PIKE MIRacle ATR designed with single frustrated internal full reflection of the germanium crystal. The results were processed by means of the software OPUS 7.2.139.1294 produced by Bruker. The magnetic parameters were measured in a constant magnetic field by means of a vibrating sample magnetometer in the measuring system Quantum Design.

The properties of the MNPs CZFO and MNCs CZFO@PEG were studied using Mössbauer spectroscopy that is an informative method for material investigation [33–37]. The Mössbauer spectra (MS) were obtained on the isotope ^{57}Fe with recording γ-radiation in a geometry of transmission through the sample under study. In order to measure the Mössbauer effect, the samples were packed in a plastic container so as to avoid interaction with the surrounding atmosphere. The source of γ-quanta ^{57}Co with activity of 50 mCi in the Rhodium matrix (Rh) in a Doppler modulator of the spectrometer was controlled via a triangular reference signal to specify a constant-acceleration speed. The speed scale was calibrated using ferrum α-foil at room temperature, and for a higher accuracy the calibration was carried out using a laser interferometer. The MS of the samples under study were obtained at room temperature. The MS were mathematically processed by a software program [38] that describes spectral lines by Lorentz-shaped using the least-square method.

Divergence of the theoretical values of the parameters of the hyperfine interactions (HFI) is determined from the statistical deviations. The software procedure of chi-square ($\chi 2$) functional minimization includes searching optimal values of the parameter, particularly, a width, intensities and positions of the spectral lines along the speed scale. Using the positions of the spectral lines, values the parameters of the hyperfine interactions were calculated: IS — the isomer

shift, QS — the quadrupole splitting, H_{eff} — the effective magnetic field. The values of the isomer shifts (IS) are given in relation to α-Fe.

3.2. X-ray-structure analysis of the MNPs $Co_{1-x}Zn_xFe_2O_4$ and MNCs $Co_{1-x}Zn_xFe_2O_4$@PEG

The X-ray diffraction patterns (XP) of the MNPs CZFO are shown on Figure 1. The lines observe at $2\theta = 30.14$, 35.49, 43.12, 53.52, 57.03 and 62.63°, designated by (220), (311), (400), (422), (511) and (440), respectively, are well matched with Miller indices of the cubic spinel structure of the $Fd3m$ space group and similar to those presented on the cards of the International Center for Diffraction Data (ICDD) for $CoFe_2O_4$ (ICDD № 00-022-1086) and CZFO (ICDD № 98-016-6201 through −6204). All the diffraction lines are widened due to the nanocrystalline nature of the ferrite particles. No additional line on the XP means a single-phase nature of the synthesized particles. The sizes of the nanoparticle crystallites, which are calculated by the most intensive line (311) of X-ray diffraction analysis by the Scherrer formula, are given in dependence on the value of the Zn ion substitution [32] in Table 1.

With increase in substitution of the cobalt ions with zinc cations, the crystallite size is reduced. It agrees with the results observed in the studies, for example, in [39–44], but does not coincide with the results obtained in the paper [45], which say that with increase in substitution with Zn ions the sizes of the particles CZFO increase. The XPs of the PEG-functionalized MNPs CZFO (not shown here) are different from those of Figure 1 by a reduced signal-to-noise ratio caused by a PEG layer of the particle surface. Functionalization of the MNPs CZFO with polyethylene glycol does not result in change of the MNP phase composition in the composites CZFO@PEG.

3.3. IR-Fourier-spectroscopy of the MNPs $Co_{1-x}Zn_xFe_2O_4$ and composites $Co_{1-x}Zn_xFe_2O_4$@PEG

Raman scattering spectroscopy (RS) is a means for investigating the properties of the ferrospinels [46,47] and makes it possible to characterize presence of the PEG layer on the particle surface. Figure 2 shows the RS spectra of the MNPs $Co_{0.6}Zn_{0.4}Fe_2O_4$, the composite $Co_{0.6}Zn_{0.4}Fe_2O_4$@PEG and PEG, which are taken at room temperature within the range of the wave numbers 500−4000 cm^{-1} at the excitation wavelength of 532 nm created by a solid-state laser. It should be noted that the RS spectra of PEG and MNPs CZFO@PEG are similar to those observed in the studies 48-50.

Figure 2 shows the spectrum of particles of the PEG-modified ferrite $Co_{0.6}Zn_{0.4}Fe_2O_4$. The spectrum consists of spectral bands belonging to a PEG organic component and bands belonging to an inorganic component of the sam-

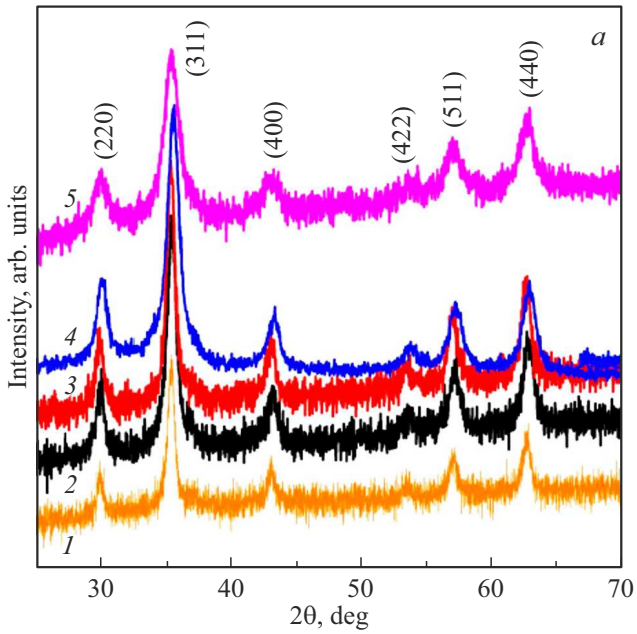

Figure 1. *a* — X-ray patterns of the nanoparticles $Co_{1-x}Zn_xFe_2O_4$. The numbers *1, 2, 3, 4* and *5* denote X-ray patterns of ferrites with Zn^{2+} ion substitutions at $x = 0.0$, 0.1, 0.2, 0.4 and 0.6, respectively.

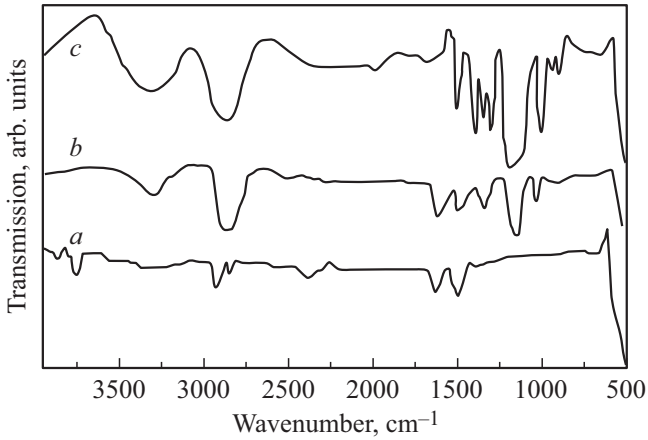

Figure 2. IR-Fourier spectra *a* — MNPs $Co_{0.6}Zn_{0.4}Fe_2O_4$, *b* — composites $Co_{0.6}Zn_{0.4}Fe_2O_4$@PEG and *c* — PEG.

Table 1. Average sizes of the crystallites, lattices constants and the blocking temperatures of the ferrites $Co_{1-x}Zn_xFe_2O_4$ depending on the number of the ions Zn^{2+}

Composition (x)	Average sizes (nm)	Lattice constant (Å)	Blocking temperature (K)
0.0	13.4	8.452	> 400
0.1	12.1	8.412	> 400
0.2	10.1	8.393	368.8
0.4	9.2	8.371	276.7
0.6	7.0	8.398	150.9

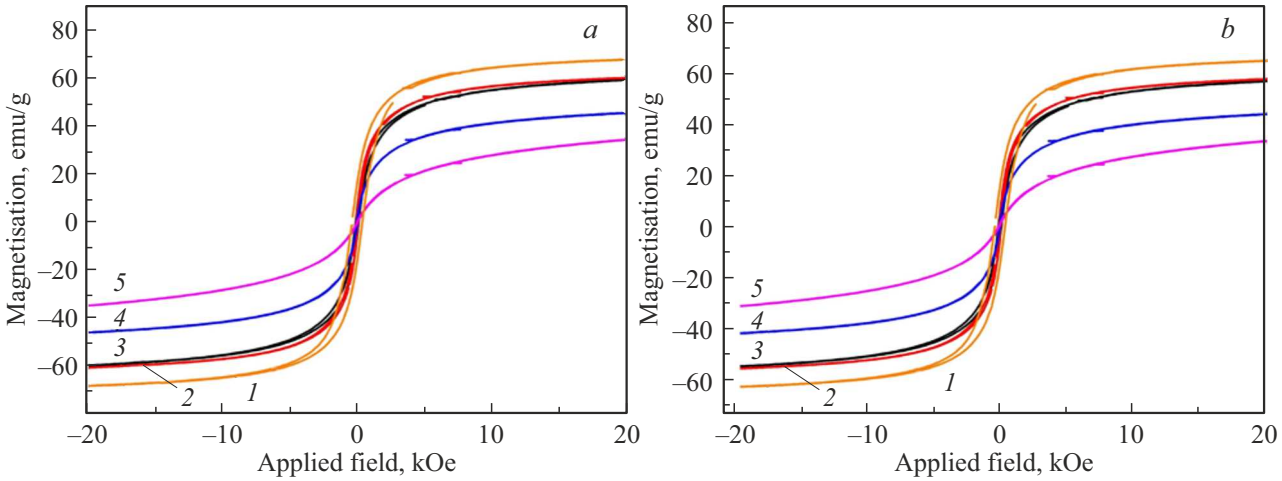

Figure 3. Magnetic characteristics obtained at room temperature within the field range from −2.0 T to +2.0 T for *a* — MNPs $Co_{1-x}Zn_xFe_2O_4$ and *b* — composites $Co_{1-x}Zn_xFe_2O_4$@PEG. Here, the numbers *1, 2, 3, 4* and *5* denote the curves obtained for the Zn^{2+} ion substitutions at $x = 0.0$, 0.1, 0.2, 0.4 and 0.6, respectively.

ple — MNPs $Co_{0.6}Zn_{0.4}Fe_2O_4$. The PEG spectrum is characterized by the spectral bands, which can be predominantly related to valence and deformation modes of vibrations of the C-H bonds (within the spectrum region 3000−2600, 1500−1250 and 950−840 cm^{-1}), as well as the modes of vibration of the C-O bonds (1200−1000 cm^{-1}) of the ether group. The RS spectra for PEG also exhibit typical vibrations at 3250 cm^{-1} (extension of −OH). It can be noted that there is certain shift of the spectral lines of both the components within the regions 1700−1700 and 1100−940 cm^{-1}. So, it can be concluded that PEG is formed on the surface of the particles $Co_{0.6}Zn_{0.4}Fe_2O_4$ by forming the Fe-O-C bonds. The simultaneous presence of the lines belong to PEG and the particles CZFO on the RS spectra of the composite $Co_{0.6}Zn_{0.4}Fe_2O_4$@PEG also confirms the bonds of PEG and the particles of the ferrite CZFO.

3.4. Magnetic properties of the MNPs $Co_{1-x}Zn_xFe_2O_4$ and the composites $Co_{1-x}Zn_xFe_2O_4$@PEG

Figure 3, *a* and *b* shows the dependences of saturation magnetization (M_S) on the content of the Zn^{2+} ions, which are obtained at room temperature when applying the external magnetic field (EMF) within the range from −2.0 to +2.0 T for the MNPs CZFO and the composites CZFO@PEG, respectively. The particles $Co_{1-x}Zn_xFe_2O_4$ with = 0.0 have maximum saturation magnetization, which decreases as the concentration of the Zn^{2+} ions increases. The dependences of magnetization on the temperature of the samples $Co_{1-x}Zn_xFe_2O_4$ inside EMF of the value of 1 T demonstrate the phase transition from the superparamagnetic into the magnetic-ordered state with decrease in the temperature within the range 5−400 K [12]. The particles $Co_{1-x}Zn_xFe_2O_4$ of the composition $x = 0.1$ and 0.2 demonstrate low coercive forces, whereas at $x = 0.4$ and 0.6 the compositions have zero coercivities and zero magnetizations. With decrease in temperature, a considerable increase in magnetization and magnetization is observed. As can be seen on Figure 3, the MS values for the composites CZFO@PEG are lower, which can be explained by impact of polyethylene glycol.

3.5. Mössbauer studies of the MNPs $Co_{1-x}Zn_xFe_2O_4$ and the MNC $Co_{1-x}Zn_xFe_2O_4$@PEG

The experimental Mössbauer spectra (MS) for the ^{57}Fe MNPs CZFO and the composites CZFO@PEG, as recorded at room temperature, are shown on Figure 4, *a* and *b*, respectively. The experimental values are dotted on Figure 4, *a* and *b*, while the model values obtained in the mathematical processing of the experimental Mössbauer spectra by means of the software program [38], are shown there by the solid lines. Good compliance of the used models with the experimental Mössbauer spectra is confirmed by minimum values of the difference between the model and experiment values, which are shown above each spectrum and by the values of $\chi 2$ within 1.0−1.2. As can be seen from Figure 4, *a* and *b*, the Mössbauer spectra are composed of lines of the Zeeman sextuplets (ZS) asymmetric towards the zero speed. The Mössbauer spectra of the MNPs CZFO (Figure 4, *a*) are similar to those observed for CZFO at the respective numbers of the Zn ions (see [12] and references therein). With increase in concentration of the Zn ions from $x = 0.1$ on the MS of the MNPS CZFO and at $x = 0$ on the MS of the MNC CZFO@PEG, there are the doublet lines appearing against the ZS background within the region of zero speed, whose intensity increases grows as the number of the Zn ions increases.

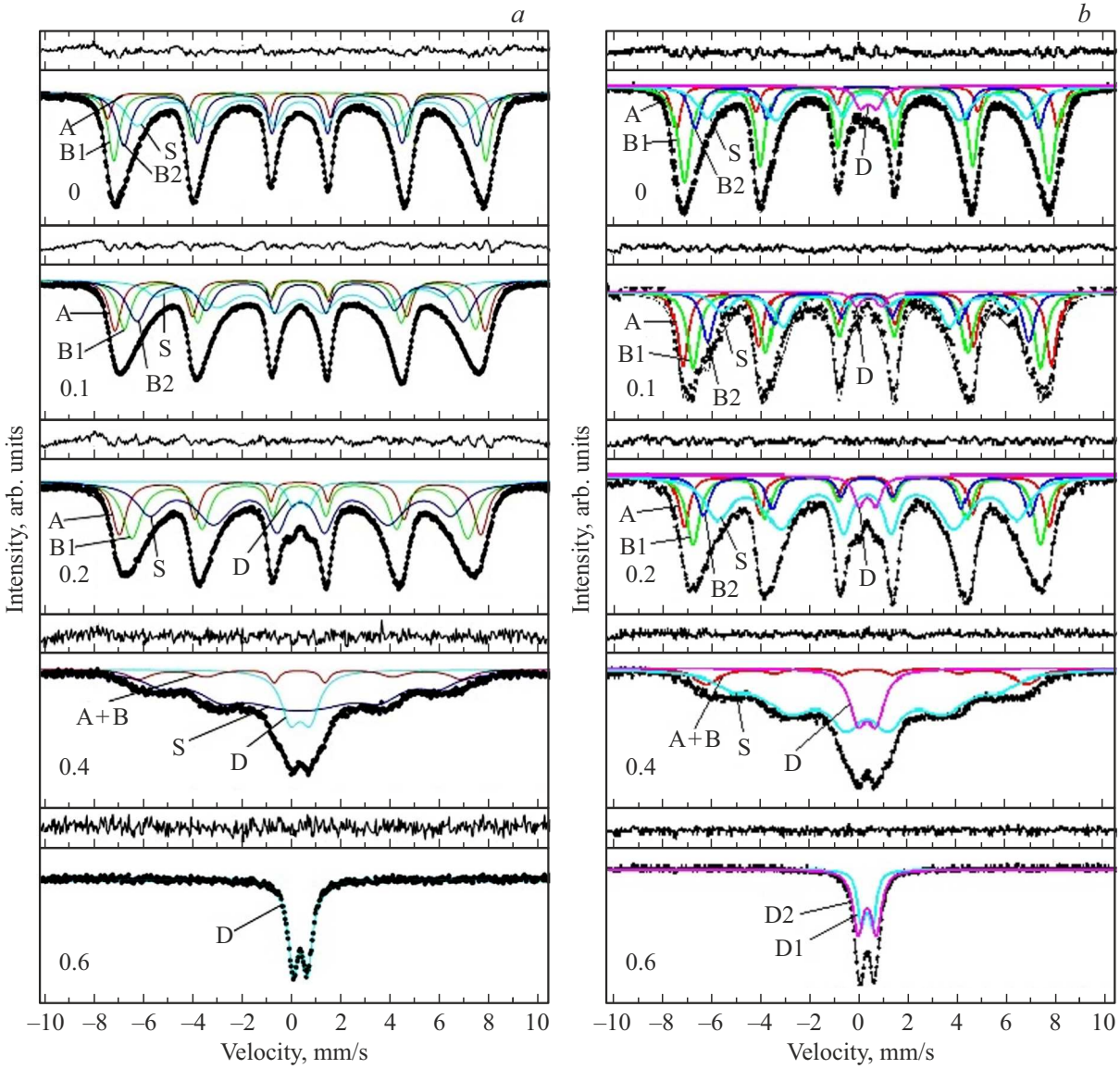

Figure 4. Room-temperature Mössbauer spectra of MNPs (*a*) $Co_{1-x}Zn_xFe_2O_4$ and MNCs (*b*) $Co_{1-x}Zn_xFe_2O_4$@PEG. The experimental value are dotted, while the model components are shown by solid color lines: The sextuplets belonging to the Fe ions in the A positions are designated by the letter A, so are they in the B positions — B1, B2, so is the paramagnetic doublet — D, S — the sextuplet of the Fe ions occupying the positions in the surface layer.

The parameters of hyperfine interactions (HFI) in Tables 2 and 3 are calculated using the position of the spectral lines in Mössbauer spectra as shown on the figures 4, *a* and 4, *b*, respectively. The isomer shifts (IS) are shown in relation to the α-Fe metal foil. The spectra of the MNPs CZFO and the MNCs CZFO@PEG under study exhibit neither additional Zeeman spectra nor doublets, with different HFI parameter belonging to the impurity (secondary) phases of the ferrum oxides. No impurity means that the materials under study are of a single-phase, which agrees with the XPs and the Raman studies.

As in Figure 4, *a, b* and in the most published studies of the spinel ferrites, the Mössbauer spectra are composed of the ZS lines asymmetric towards the zero speed. This shape is explained by formation Zeeman sub-spectra on the Mössbauer spectra of the spinel ferrites. Their line intensity and efficiency magnetic fields (H_{eff}) depend on the probability of distribution of the Fe atoms and the metal ions (M) doped in MFe_2O_4 across the non-equivalent positions of the crystal lattice. The probability of this distribution is described by a binomial function [51,52]. Based on the above-said and analysis of the Mössbauer spectra of the spinel ferrites [12,33], the Mössbauer spectra of the MNPs CZFO and the MNCs CZFO@PEG were processed using the sextuplets and the doublets, thereby enabling obtaining satisfactory compliance of the experimental Mössbauer spectra with the model in terms of a criterion $\chi 2$.

Table 2. Obtained for the MNPs $Co_{1-x}Zn_xFe_2O_4$: the widths of the first and sixth lines (G) of the Zeeman splitting, the isomer shifts (IS), the quadrupole splittings (QS), the effective magnetic fields (H_{eff}) and the areas of the lines (In) of the Fe ions in the tetrahedral (B), octahedral [A] positions, in the surface layer (S) and the doubles (D) depending on substitution with the Zn (x) ions

x	Compon.	G (mm/s)	IS (mm/s)	QS (mm/s)	H_{eff} (T)	In (%)
0.0	A	0.447 ± 0.026	0.321 ± 0.002	0.028 ± 0.004	48.12 ± 0.06	21
	B1	0.553 ± 0.039	0.309 ± 0.002	0.009 ± 0.003	46.26 ± 0.05	8
	B2	0.650 ± 0.055	0.315 ± 0.002	0.017 ± 0.004	44.01 ± 0.07	29
	S	1.222 ± 0.031	0.338 ± 0.004	0.017 ± 0.008	40.96 ± 0.15	42
0.1	A	0.505 ± 0.016	0.315 ± 0.001	0.019 ± 0.003	46.91 ± 0.04	12
	B1	0.615 ± 0.029	0.303 ± 0.001	0.017 ± 0.003	44.84 ± 0.04	18
	B2	0.897 ± 0.039	0.319 ± 0.002	-0.004 ± 0.003	42.04 ± 0.05	27
	S	1.231 ± 0.028	0.332 ± 0.003	0.020 ± 0.005	37.77 ± 0.11	43
0.2	A	0.688 ± 0.020	0.309 ± 0.002	0.020 ± 0.003	45.41 ± 0.04	19
	B	0.933 ± 0.049	0.303 ± 0.002	0.020 ± 0.004	42.21 ± 0.06	32
	S	1.322 ± 0.032	0.343 ± 0.004	0.019 ± 0.007	37.83 ± 0.12	45
	D	0.564 ± 0.024	0.343 ± 0.005	0.649 ± 0.012	–	4
0.4	A+B	1.125 ± 0.135	0.314 ± 0.010	0.013 ± 0.020	40.51 ± 0.27	11
	S	1.560 ± 0.221	0.338 ± 0.013	0.005 ± 0.020	34.62 ± 0.39	70
	D	0.915 ± 0.027	0.331 ± 0.004	0.794 ± 0.011	–	19
0.6	D	0.503 ± 0.006	0.336 ± 0.002	0.576 ± 0.004	–	100

Table 3. Obtained for the composites $Co_{1-x}Zn_xFe_2O_4$@PEG: the widths of the first and sixth lines (G) of the Zeeman splitting (IS), the quadrupole splittings (QS), the effective magnetic fields (H_{eff}) and the areas of the lines (In) of the Fe ions in the tetrahedral (B), octahedral [A] positions, in the surface layer (S) and the doublets (D) depending on substitution with the Zn (x) ions

x	Compon.	G (mm/s)	IS (mm/s)	QS (mm/s)	H_{eff} (T)	In (%)
0.0	A	0.406 ± 0.016	0.333 ± 0.002	-0.007 ± 0.005	48.15 ± 0.02	12
	B1	0.618 ± 0.019	0.310 ± 0.001	-0.013 ± 0.002	46.05 ± 0.01	41
	B2	0.572 ± 0.000	0.325 ± 0.003	-0.002 ± 0.005	43.32 ± 0.04	14
	S	1.077 ± 0.028	0.344 ± 0.004	0.028 ± 0.007	40.15 ± 0.06	29
	D	0.578 ± 0.000	0.394 ± 0.008	0.626 ± 0.012	–	4
0.1	A	0.525 ± 0.000	0.314 ± 0.005	-0.048 ± 0.011	46.57 ± 0.05	26
	B1	0.578 ± 0.000	0.322 ± 0.006	-0.000 ± 0.011	43.82 ± 0.07	33
	B2	0.582 ± 0.000	0.350 ± 0.009	-0.062 ± 0.018	40.39 ± 0.09	19
	S	0.920 ± 0.000	0.287 ± 0.021	0.025 ± 0.041	36.29 ± 0.19	19
	D	0.563 ± 0.000	0.416 ± 0.041	0.972 ± 0.072	–	3
0.2	A	0.542 ± 0.091	0.311 ± 0.006	-0.020 ± 0.012	46.10 ± 0.19	15
	B1	0.682 ± 0.168	0.303 ± 0.006	-0.030 ± 0.012	43.81 ± 0.21	22
	B2	0.621 ± 0.000	0.317 ± 0.009	0.005 ± 0.018	41.15 ± 0.20	14
	S	1.243 ± 0.086	0.345 ± 0.010	-0.001 ± 0.019	37.74 ± 0.29	45
	D	0.557 ± 0.072	0.348 ± 0.018	0.654 ± 0.038	–	4
0.4	A + B	1.272 ± 0.112	0.320 ± 0.022	0.028 ± 0.046	40.29 ± 0.20	11
	S	1.483 ± 0.155	0.315 ± 0.017	0.021 ± 0.030	33.73 ± 0.34	74
	D	0.838 ± 0.048	0.328 ± 0.007	0.712 ± 0.023	–	15
0.6	D1	0.369 ± 0.023	0.326 ± 0.002	0.421 ± 0.020	–	38
	D2	0.498 ± 0.007	0.338 ± 0.002	0.708 ± 0.028	–	62

As can be seen from Tables 2 and 3, the IS vales of the Fe ions in the [B] and (A) positions are almost the same and do not depend on the number of the Zn ions, thereby indicating insensitivity of the s-electrons of the Fe^{8+} ions to the quantity of Zn. The spectral lines of Fe^{2+} and Fe^{8+} are reliably identified in Mössbauer spectroscopy by their chemical shifts, which are $\sim 0.2-0.5$ mm/s for Fe^{8+} and $\sim 0.9-1.1$ mm/s for Fe^{2+} [14]. In the materials under study, the IS values for the Fe ions in the A and B positions are within 0.3–0.5 mm/s (Tables 2 and 3). It indicates that the samples have only high-spin ferrum ions Fe^{8+}, whereas the low-spin ions Fe^{2+} are absent. The QS values (Tables 2

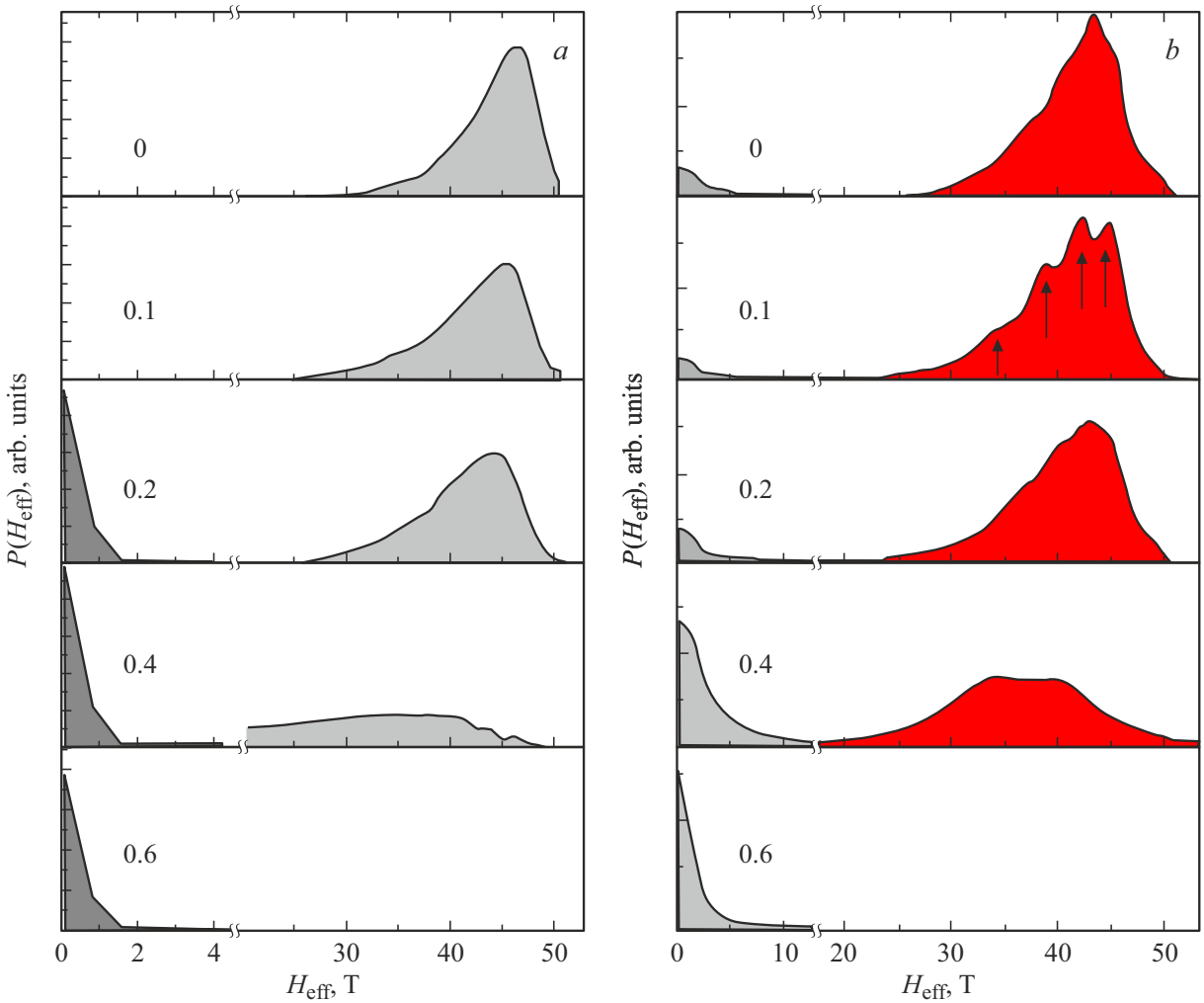

Figure 5. Distribution functions $P(H_{\text{eff}})$ *a* — the MNPs $Co_{1-x}Zn_xFe_2O_4$ and *b* — the MNCs $Co_{1-x}Zn_xFe_2O_4$@PEG, which are reconstructed from the experimental Mössbauer spectra using the software program [65].

and 3) are close to zero (except for QS for the doublets), thereby indicating preservation of the cubic symmetry of the Fe^{8+} ions and its environment. The QS values of the doublets below 0.8 mm/s also mean that the Fe ions are in the high-spin state Fe^{8+}, since for the ions of the low-spin Fe^{2+} the QS values are substantially higher.

The Mössbauer spectra of the MNPs CZFO at $x = 0$ against the ZS background at $x = 0.2$ exhibit a doublet, whose intensity with increase in the number of the Zn ions increases, while the intensity of the ZS decreases, and at $x = 0.6$ there is only a paramagnetic doublet observed. These changes of the Mössbauer spectra of the MNPs CZFO are explained by superparamagnetic relaxation [54,55]. If the relaxation time (τ) of the nanoparticles is less than the measurement time ($\tau_M = 10^{-7}$ s for ^{57}Fe), then the Mössbauer spectra are composed of a doublet. At $\tau \gg \tau_M$, the Mössbauer spectra exhibit the Zeeman spectrum with good resolution of the absorption lines. The blocking temperature (T_{PB}) is determined from the Mössbauer spectrum as a temperature, where the areas of the sextuplets and the paramagnetic doublet are equal to each other. The results of the analysis of the areas of the spectral lines of the components in the Mössbauer spectra of the MNPs CZFeO (Table 2) make it possible to state that with increase in the content of the Zn ions T_{B} decreases and at $x = 0.6$ it becomes lower than the room temperature, which agrees with the data of magnetic measurements. As can be seen on Figure 5, *a, b*, in addition to the sextuplets (A) and [B], the Mössbauer spectra of the MNPs CZFO also have the Zeeman spectra, which are designated by S on Figure 5, *a*, whose line widths are significantly bigger. Let us consider the causes of formation of the S sextuplet in the Mössbauer spectrum of MNPs CZFO.One of the causes may include contributions of the Fe ions, a number of the immediate neighbors thereof is less than for the ferrum ions in the B1 and B2 positions. Another cause may be the fact that with decrease in the particle size the surface/volume ratio increases multiple times, thereby substantially increasing a MS portion from the ferrum ions, which occupy the positions in the MNP surface layer and

lost a part of the immediate magnetic neighbors (a part of superexchange interactions) because of the surface [56]. It explains formation of the canted spin structure in the surface layer of the MNPs or the „magnetic-dead" or spin-glass surface layer, which reduce magnetization and the temperature of the MNP magnetic ordering (see [12,56,57] and references therein). Existence of the collinear (Neel) ordering in the nanoparticles of the ferrites MFe_2O_4 is proved by the Mössbauer studies in the large EMFs [59–61].

Existence of the canted spin structure in the surface layer of the macroscopic crystals of the hexagonal ferrites was proven for the first time in the study [62] using a new unique procedure, which is developed by the authors [63], „for Mössbauer studies of the properties of the surface layer and the bulk simultaneously" without EMF use. Based on the results of the studies (see [62] and references therein), it can be assumed that with decrease in the crystal size the canted spin structure in the surface layer is not only preserved, but its thickness increases. Therefore, the data of the Mössbauer studies make it possible to state that the surface layer of the MNPs CZFO and the MNCs CZFO@PEG has the canted magnetic structure.

3.6. Distribution functions H_{eff} for the MNPs $Co_{1-x}Zn_xFe_2O_4$ and MNCs $Co_{1-x}Zn_xFe_2O_4$@PEG

In case of no ZS resolution, the most reliable is the MS analysis method using the function V_{oigt} as a spectral line [64,65].For this reason, using the software program [38] having the Voigt function, the experimental Mössbauer spectra were taken to reconstruct therefrom functions of probabilities of distribution of the effective fields $P(H_{\text{eff}})$, which are shown on Figure 5, *a* and *b*. The obtained functions $P(H_{\text{eff}})$ differ from the curve $P(H_{\text{eff}})$ of the SF macrocrystals, which evidently only two maximums belonging to the ferrum ions in the non-equivalent sublattices (A) and [B]. The Mössbauer spectra of the MNPs and the composites (Figure 4, *a* and *b*) slightly differ from each other, whereas the distribution functions $P(H_{\text{eff}})$ of the MNPs CZFO and the MNCs CZFO@PEG, as shown on Figure 5, *a* and *b*, are different.

In case of the MNPs CZFO at $x \leq 0.4$ (Figure 5, *a*) within the field region from 47 to 43 T, the functions $P(H_{\text{eff}})$ monotonously increase and after the maximum they decrease monotonously as well. Asymmetry of the curves $P(H_{\text{eff}})$ towards smaller H_{eff} observed within the region from 45 T and below is explained by decrease in the number of the magnetic ions in the immediate environment of the Fe ions. On the Mössbauer spectrum, the region from 0 to 1.6 T corresponds to the doublet lines that indicate presence of paramagnetic-state particles in the sample. With increase in the number of the Zn ions (Figure 5, *a*) the H_{eff} values decrease, a position of the maximum H_{eff} is shifted towards smaller fields and the portion of the magnetic-ordered phase is reduced. At the same time, the intensities of the paramagnetic-phase lines increase and when substitution (x) is 0.6, the function $P(H_{\text{eff}})$ retains only a line that corresponds to the paramagnetic state of the MNPs. A distinctive feature that distinguishes the functions of the MNPs CZFO@PEG from $P(H_{\text{eff}})$ for the MNPs CZFO is that the paramagnetic phase is observed across the entire range of substitutions by the Zn ions. Another important difference is that the functions $P(H_{\text{eff}})$ for the MNPs CZFO change smoothly, whereas in case of the MNCs CZFO@PEG there is non-monotonous change and it can be described by separate lines, which are shown on Figure 5, *b* by arrows for the composite $x = 0.1$ as an example. This indicates differences of local environments of the ferrum atoms in the particles that are coated and uncoated with a surfactant layer. The description of the function $P(H_{\text{eff}})$ for the MNCs CZFO@PEG by the separate lines means formation of small PEG-coated clusters in the composites, thereby resulting in reduction of interaction between the clusters, whereas in the uncoated MNPs the particles interact with each other [66].

The polyethylene glycol is a film designed to reduce/prevent interaction in the MNCs CZFO@PEG between separate clusters, whose properties depend on the cluster size, the particle size and the substitution by the Zn ions in the cluster.

The assumption that the coating reduces interaction between the particles was confirmed by Mössbauer studies of the coated and uncoated particles before and after pressing [67,68]. Thus, in case of the maghemite particles of the size of 7 nm the effective magnetic fields increase after pressing [67]. It is explained by compaction of the uncoated MNPs, the reduced interparticle distance that results in increase in interactions between the nanoparticles and, therefore, growth of the effective magnetic fields. The obtained Mössbauer spectra of the coated sample before and after pressing had the same parameters of hyperfine interactions, i. e., they were unchanged, as the coating molecules prevent closing of the separate clusters being formed during functionalization and, therefore, enhancement of exchange interactions. The pressing of the uncoated MNPs α-Fe_20_3 of the size of 7 nm suppresses superparamagnetic relaxation, which was explained by enhancement of the exchange interactions with reduction of the interparticle distance [68].

3.7. Evaluation of the MNP sizes in $Co_{1-x}Zn_xFe_2O_4$ and in MNC CZFO@PEG

The experimental Mössbauer spectra of the MNPs CZFO were analyzed and compared with the published Mössbauer data so as to evaluate the size of the nanoparticles under study [12]. As a result, it has been established that the sizes of the MNPs CZFO decreased from 14 to 8 nm with increase in the Zn content from $x = 0$ to $x = 0.6$. The obtained values agree with the X-ray diffraction data. The Mössbauer spectra of the MNCs $Co_{1-x}Zn_xFe_2O_4$@PEG have been analyzed to show that both the coated and the uncoated magnetic nanoparticles have almost the same sizes.

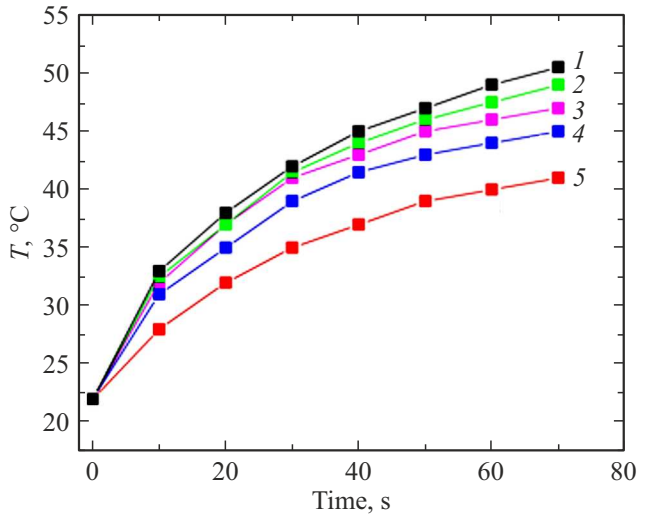

Figure 6. Dependences of the temperature of $Co_{1-x}Zn_xFe_2O_4$@PEG ($0 \le x \le 0.6$) on the time of heating by the variable magnetic field of frequency of 2.0 MHz and the strength of 4.5 kA/m. The numbers *1, 2, 3, 4* and *5* denote the concentrations of the Zn ions (x), which are 0, 0.1, 0.2, 0.4 and 0.6, respectively.

3.8. Hyperthermia studies of the MNCs $Co_{1-x}Zn_xFe_2O_4$@PEG

Figure 6 shows the change of the aqueous solution temperature of the MNCs CZFO@PEG with the different Zn content depending on the time of heating by the external variable magnetic field (EVMF) of the frequency of 2.0 MHz and strength of 4.5 kA/m. As can be seen on Figure 6, the maximum achievable temperature depends on the Zn content. It is clear that with increase in the number of the Zn ions, the temperature of the particles increases. The PEG-functionalized MNPs CZFO obtain the hyperthermia temperature for the short time interval at small concentrations of the Zn ions ($0 \le x \le 0.4$). The obtained dependences (Figure 6) agree with the results of the papers, like in [14].

Figure 7 shows the change of the specific absorption rate of the aqueous solution of the MNCs CZFO@PEG depending on the strength of EVMF of the fixed frequency of 2.0 MHz. It is reported in the literature [22,23] that the linear SAR change with EVMF application may be related to the chemical composition of the ferrofluid. The particle sizes substantially affect the value of the specific absorption rate. In case of the MNC $CoFe_2O_4$@PEG of the size of 14 nm, the maximum SAR 52.2 W/g was achieved in the magnetic field of 4.5 kA/m, whereas in EVMF of the strength of 2 kA/m it was reduced to 14.2 W/g. For the finer particles $Zn_{0.6}Co_{0.4}Fe_2O_4$ PEG of the size of about 8 nm, the SAR values did not exceed 34 W/g at the variable field of 4.5 kA/m and 5 W/g for the field of 2 kA/m.

Another important factor, on which the SAR values depend, is saturation magnetization. There is noticeable increase in the values of the specific absorption rate with increase in the saturation magnetization. For the particles $Co_{0.4}Zn_{0.6}Fe_2O_4$ with the saturation magnetization of 33 emu/g, the SAR values vary within the interval from 10 to 38.1 W/g, whereas for the nanoparticles $CoFe_2O_4$ with the saturation magnetization of 68.4 emu/g the SAR values were within the range from 19.2 to 53.2 W/g depending on the value of the external magnetic field.

Figure 8 shows the specific absorptions (SAR) of the aqueous solution of the MNCs CZFO@PEG depending

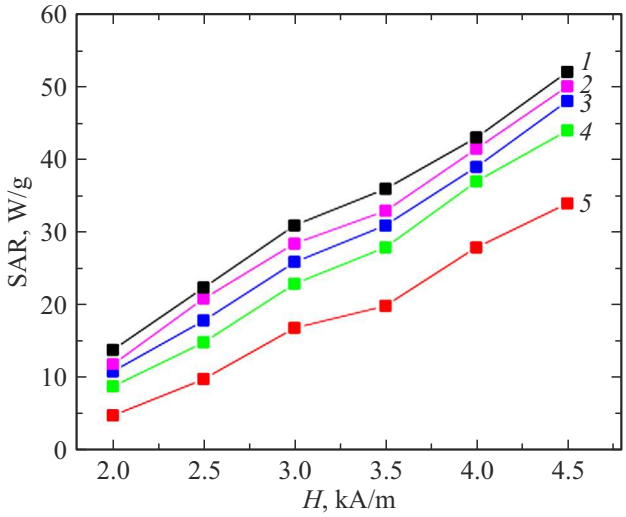

Figure 7. Specific absorption rate of the aqueous solution of MNCs $Co_{1-x}Zn_xFe_2O_4$@PEG ($0 \le x \le 0.6$) depending on the strength of the external variable magnetic field of the frequency of 2.0 MHz. The numbers *1, 2, 3, 4* and *5* correspond to the values of x, which are 0, 0.1, 0.2, 0.4 and 0.6.

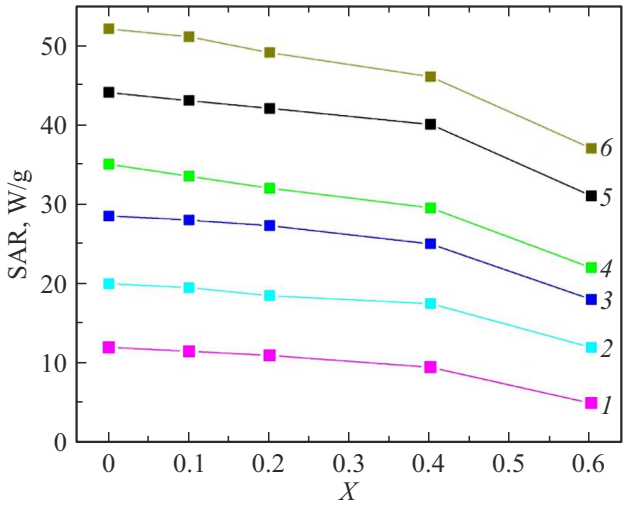

Figure 8. Dependences of the specific absorption rate of the aqueous solution of the MNCs $Co_{1-x}Zn_xFe_2O_4$@PEG on the Zn concentration at the various values of the external variable magnetic field of the frequency of 2.0 MHz. The designations *1, 2, 3, 4, 5* and *6* correspond to the values of the external fields, which are 2, 2.5, 3.0, 3.5, 4.0 and 4.5 kA/m.

on the Zn concentration at the various values of EVMF of the frequencies of 2.0 MHz. The SAR values decrease with increase in substitution of cobalt with the zinc cations. Figure 8 exhibits an almost linear change of the SAR value, whereas for the nanoparticles $CoFe_2O_4$ with the saturation magnetization of 62.4 emu/g the SAR values were within the range from 10.2 to 52.2 W/g. The similar curves have been obtained in the studies [69,70] and linearity of the SAR value dependences was related to the chemical composition of the ferrofluid.

Analyzing the results, the maximum SAR value of 52.2 W/g was achieved in case of the composite $CoFe_2O_4$@PEG with application of EVMF of the strength of 4.5 kA/m, thereby making it a promising candidate for hyperthermia therapy of malignant tumors. Studying the SAR values makes it possible to observe its dependence on the chemical composition, the size of the particles, the saturation magnetization and the value of the external variable magnetic field.

4. Conclusion

The properties of the MNPs $Co_{1-x}Zn_xFe_2O_4$ ($x = 0.0, 0.1, 0.2, 0.4, 0.6$) (synthesized by the codeposition method) and impact of functionalization (coating) with polyethylene glycol have been systematically investigated. The structural and morphological properties of the MNPs have been studied using X-ray diffraction (XD), magnetic measurements, Raman spectroscopy and Mössbauer spectroscopy (MS). The structural XD analysis as well as the data of the Raman spectroscopy and Mössbauer spectroscopy confirm the single-phase nature of the particles under study both before PEG functionalization and after it. It has been established that the MNPs had the cubic structure of the spinel ferrite $Co_{1-x}Zn_xFe_2O_4$ (the spatial group $Fd3m$) across the entire range of substitution by the Zn ions.

Based on the X-ray diffraction and Mössbauer data, it has been established that the average sizes of the crystallites $Co_{1-x}Zn_xFe_2O_4$ decreased from 14 to 8 nm with increase in the portion of the Zn ions from 0 to 0.6. The functionalization of the MNPs $Co_{1-x}Zn_xFe_2O_4$ with polyethylene glycol has almost no change of the sizes of the magnetic particles in the composites $Co_{1-x}Zn_xFe_2O_4$@PEG. The experimental Mössbauer spectra indicate the typical superparamagnetic behavior of the MNPs $Co_{1-x}Zn_xFe_2O_4$ and the composites $Co_{1-x}Zn_xFe_2O_4$@PEG. With increase in the Zn concentrations $x > 0.1$, the thin surface layer of the particles $Co_{1-x}Zn_xFe_2O_4$ exhibits the paramagnetic state. With increase in the number of the Zn ions, the thickness of this surface layer increases and at $x = 0.6$ the entire particle becomes paramagnetic. It has been shown that the bulk of the MNPs CZFO and the MNCs CZFO@PEG exhibited collinear ordering of the spin moments, whereas in the surface layer the spin moments had the canted structure due to surface impact. Thus, the information obtained in the studies [12,57] is confirmed, wherein these studies are the first ones establishing the differences of the magnetic structure of the bulk and the surface layer of the magnetic nanoparticles by means of the Mössbauer spectroscopy, without the external magnetic field.

Decomposability of the function $P(H_{\text{eff}})$ for the MNCs CZFO@PEG into separate peaks means that the particles, which are approximately the same in size, are formed in the MNC in the clusters, which are covered by the surfactant. Polyethylene glycol in the MNCs CZFO@PEG is a film designed to reduce/prevent interaction between the separate clusters, and the distribution functions H_{eff} exhibit peaks from these clusters. In the uncoated MNPs, all the particles interact between each other and the distribution functions of the effective fields change smoothly.

The obtained results are important for designing the magnetic nanoparticles, their functionalization and creating the magnetic nanocomposites for various applications, including biomedical ones.

Conflict of interest

The authors declare that they have no conflict of interest.

References

[1] Ferrite Nanostructured Magnetic Materials Technologies and Applications / Ed. Jitendra Pal Singh, Keun Hwa Chae, Ramesh Chandra Srivastava, Ovidiu Florin Caltun. 1st ed. Woodhead Publishing (2023). 926 p.
[2] Magnetic Nanoparticles for Biomedical Applications / Ed. Martin F. Desimone, Rajshree B. Jotania. Publ. Mater. Res. Forum LLC. USA (2023). 316 p.
[3] A. Mittal, I. Roy, S. Gandhi. Magnetochemistry **8**, 107 (2022). https://doi.org/10.3390/magnetochemistry8090107.
[4] M. Hepel. Magnetochemistry **6**, 3 (2020). DOI: 10.3390/magnetochemistry6010003
[5] V. Socoliuc, D. Peddis, V.I. Petrenko, M.V. Avdeev, D. Susan-Resiga, T. Szabó, R. Turcu, E. Tombácz, L. Vékás. Nanoscale **14**, 4786 (2022). DOI: 10.1039/d1nr05841j.
[6] S.I. Ahmad. J. Magn. Magn. Mater. **562**, 169840 (2022). https://doi.org/10.1016/j.jmmm.2022.169840
[7] B. Pacakova, S. Kubickova, A. Reznickova, D. Niznansky, J. Vejpravova. Spinel Ferrite Nanoparticles: Correlation of Structure and Magnetism. In: Magnetic Spinels — Synthesis, Properties and Applications. TechOpen / Ed. M.S. Seehra. (2017). Ch. 1. P. 4–29. DOI: 10.5772/66074.
[8] M.G. Goodarz, E.B. Saion, M.H. Hashim, A.H. Shaari, H.A. Ahangar. Solid State Commun. **15**, 1031 (2011). https://doi.org/10.1016/j.ssc.2011.04.018.
[9] E.C. Mendonca, C.B.R. Jesus, C.T. Meneses, J.G.S. Duque. J. Supercond. Nov. Magn. **26**, 2329 (2013). DOI: 10.1007/s10948-012-1426-3.
[10] G. Vaidyanathana, S. Sendhilnathan. Physica B **403**, 2157 (2008).
[11] A.S. Kamzin, D.S. Nikam, S.H. Pawar. Phys. Solid State **59**, *1*, 156 (2017). https://link.springer.com/article/10.1134/S1063783417010127.

[12] A.S. Kamzin, I.M. Obaidat, V.G. Semenov, V. Narayanaswamy, I.A. Al-Omari, B. Issa, I.V. Buryanenko. Phys. Solid State **65**, *3*, 470 (2023). DOI: 10.21883/PSS.2023.03.55591.544.
[13] V. Narayanaswamy, I.A. Al-Omari, A.S. Kamzin, B. Issa, H.O. Tekin, H. Khourshid, H. Kumar, A. Mallya, S. Sambasivam, I.M. Obaidat. Nanomater. **11**, *5*, 1231 (2021). https://doi.org/10.3390/nano11051231
[14] A. Doaga, A.M. Cojocariu, C.P. Constantin, R. Hempelmann, O.F. Caltun. AIP Conf. Proc. **1564**, 123 (2013). DOI: 10.1063/1.4832806.
[15] M. Albino, E. Fantechi, C. Innocenti, A. López-Ortega, V. Bonanni, G. Campo, F. Pineider, M. Gurioli, P. Arosio, T. Orlando, G. Bertoni, C.D. Fernandez, A. Lascialfari, C. Sangregorio. J. Phys. Chem. C **123**, *10*, 6148 (2019). https://doi.org/10.1021/acs.jpcc.8b10998
[16] F. Sharifianjazi, M. Moradi, N. Parvin, A. Nemati, A.J. Rad, N. Sheysi, A. Abouchenari, A. Mohammadi, S. Karbasi, Z. Ahmadi, A. Esmaeilkhanian, M. Irani, A. Pakseresht, S. Sahmani, M.S. Asl. Ceram. Int. **46**, *11*, Part B, 18391 (2020).
[17] V. Socoliuc, M.V. Avdeev, V. Kuncser, Rodica Turcu, Etelka Tombácz, L. Vékás. Nanoscale **14**, 4786 (2022). https://doi.org/10.1039/D1NR05841J
[18] D.S. Nikam, S.V. Jadhav, V.M. Khot, R.S. Ningthoujam, C.K. Hong, S.S. Malic, S.H. Pawar. RSC Adv. *4*, 12662 (2014). DOI: 10.1039/c3ra47319h.
[19] C. Nayek, K. Manna, G. Bhattacharjee, P. Murugavel, I. Obaidat. Magnetochemistry **3**, 19 (2017). DOI: 10.3390/magnetochemistry3020019.
[20] A.S. Karakoti, R. Shukla, R. Shanker, S. Singh. Adv. Colloid Interface Science **215**, 28 (2015). http://dx.doi.org/10.1016/j.cis.2014.11.004.
[21] Nguyen T.K. Thanh, Luke A.W. Green. Nano Today **5**, 213 (2010). DOI: 10.1016/j.nantod.2010.05.003
[22] M. Mikhaylova, Y.S. Jo, D.K. Kim, N. Bobrysheva, Y. Andersson, T. Eriksson, M. Osmolowsky, V. Semenov, M. Muhammed. Hyperfine Interactions **156/157**, 257 (2004).
[23] K. Mažeika, V. Bėčytė, Yu.O. Tykhonenko-Polishchuk, M.M. Kulyk, O.V. Yelenich, A.I. Tovstolytkin. Lithuanian J. Phys. **58**, 267 (2018).
[24] T.J. Daou, J.M. Grene‘che, G. Pourroy, S. Buathong, A. Derory, C. Ulhaq-Bouillet, B. Donnio, D. Guillon, S. Begin-Colin. Chem. Mater. **20**, 5869 (2008).
[25] W.B. Mdlalose, S.R. Mokhosi, S. Dlamini, T. Moyo, M. Singh. AIP Advances **8**, 056726 (2018). https://doi.org/10.1063/1.5007760
[26] V. Kuncser, G. Schinteie, B. Sahoo, W. Keune, D. Bica, l. Vékás, G. Filoti. Roman. Rep. Phys. **58**, 273 (2006).
[27] V. Kuncser, G. Schinteie, B. Sahoo, W. Keune, D. Bica, l. Vékás, G. Filoti. J. Phys.: Condens. Matter **19**, 016205 (2007). DOI: 10.1088/0953-8984/19/1/016205.
[28] M. Kaur, M. Kaur, D. Singh, A.C. Oliveira, V.K. Garg, V.K. Sharma. Nanomaterials **11**, 1471 (2021). https:// doi.org/10.3390/nano11061471
[29] B. Wareppam, E. Kuzmann, V.K. Garg, L.H. Singh. J. Mater. Res. **28**, 937 (2022). DOI: 10.1557/s43578-022-00665-4.
[30] Materials Science and Materials Engineering. Comprehensive Nanoscience and Nanotechnology / Ed. S. Mørup, M.F. Hansen, C. Frandsen. Magnetic Nanoparticles. V. 1 (2019). P. 89–140. https://doi.org/10.1016/B978-0-12-803581-8.11338-4
[31] C. Frandsen, S. Mørup. Phys. Rev. Lett. **94**, 039708 (2005).
[32] M. Sajida, J. Płotka-Wasylka. Microchem. J. **154**, 104623 (2020). https://doi.org/10.1016/j.microc.2020.104623.
[33] A.S. Kamzin, I.M. Obaidat, V.G. Semenov, V. Narayanaswamy, I.A. Al-Omari, B. Issa, I.V. Buryanenko. Phys. Solid State. **64**, *6*, 714 (2022). DOI: 10.21883/PSS.2022.06.53838.298.
[34] E. Umut, M. Coskun, H. Gungunes, V. Dupuis, A.S. Kamzin. J. Supercond. Nov. Magn. **34**, *3*, 913 (2021). https://doi.org/10.1007/s10948-020-05800-y
[35] A.S. Kamzin, I.M. Obaidat, A.A. Valliulin, V.G. Semenov, I.A. Al-Omari. Phys. Solid State **62**, *11*, 2167 (2020)]. DOI: 10.1134/S1063783420110153.
[36] S. Morup, J.A. Dumesic, H. Topsøe. In: Mossbauer spectroscopy applications / Ed. R.L. Cohen. Academic, N.Y. (1990). P. 1.
[37] V. Kuncser, O. Crisan, G. Schinteie, F. Tolea, P. Palade, M. Valeanu, G. Filoti. Modern Trends in Nanoscience. Editura Academiei Romane, Bucharest (2013). V. 197.
[38] V.G. Semenov, V.V. Panchuk. Programma matematicheskoy obrabotki messbauerovskikh spectrov MossFit. Chast. soobschenie (2015). (in Russian).
[39] P.A. Rao, K.S. Rao, T.R.K.P. Raju, G. Kapusetti, M. Choppadandi, M.C. Varma, K.H. Rao. J. Alloys Comp. **794**, 60 (2019). https://doi.org/10.1016/j.jallcom.2019.04.242.
[40] M.I.A.A. Maksoud, A. El-Ghandour, G.S. El-Sayyad, R.A. Fahim, A.H. l-Hanbaly, M. Bekhit, E.K. Abdel-Khalek, H.H. El-Bahnasawy, M.A. Elkodous, A.H. Ashour, A.S. Awed. J. Inorg. Organomet. Polym. Mater. **30**, 3709 (2020). https://doi.org/10.1007/s10904-020-01523-8.
[41] D.S. Nikam, S.V. Jadhav, V.M. Khot, R.A. Bohara, C.K. Hong, S.S. Malib, S.H. Pawar. RSC Adv. *5*, 2338 (2015). https://doi.org/10.1039/c4ra08342c.
[42] M.S. Hossain, Md.B. Alam, M. Shahjahan, M.H.A. Begum, Md.M. Hossain, S. Islam, N. Khatun, M. Hossain, M.S. Alam, Md. Al-Mamun. J. Adavanc. Dielectr. **8**, *4*, 1850030 (2018). DOI: 10.1142/S2010135X18500303.
[43] K.M. Batoo, E.H. Raslan, Y. Yang, S.F. Adil, M. Khan, A. Imran, Y. Al-Douri. AIP Advances **9**, 055202 (2019); https://doi.org/10.1063/1.5078411
[44] J. Lopez, W.R. Aguirre-Contreras, M.E. Gómez, G. Zambrano. Int. J. Appl. Natur. Sci. **6**, *2*, 47 (2017).
[45] M.B. Ali, K.E. Maalam, H.E. Moussaoui, O. Mounkachi, M. Hamedoun, R. Masrour, E.K. Hlil, A. Benyoussef. J. Magn. Magn. Mater. **398**, 20 (2016). http://dx.doi.org/10.1016/j.jmmm.2015.08.097
[46] V. Bartňěk, D. Sedmidubský, Š. Huber, M. Švecová, P. Ulbrich, O. Jankovský. Materials **11**, 1241 (2018). DOI: 10.3390/ma11071241.
[47] N. Monni, V. Mameli, S.A. Sahadevan, S. Gai, C. Cannas, M.L. Mercuri. J. Nanosci. Nanotechnology **19**, 5043 (2019). DOI: 10.1166/jnn.2019.16792
[48] Y. Koseoglu, A. Baykal, M.S. Toprak, F. Gozuak, A.C. Basaran, B. Aktas. J. Alloys Comp. **462**, 209 (2008).
[49] X.H. Liu, J. Yang, L. Wang, X.J. Yang, L.D. Lu. Mater. Sci. Eng. A **289**, 7483 (2003).
[50] V.M. Khotn, A.B. Salunkhe, J.M. Ruso, S.H. Pawar. J. Magn. Magn. Mater. **384**, 335 (2015).
[51] G.A. Sawatzky, F. Van Der Woude, A.H. Morrish. Phys. Rev. **187**, *2*, 747 (1969).
[52] F. van Der Woude, G.A. Sawatzky. Phys. Rev. B **4**, *9*, 3159 (1971).

[53] Q. Lin, J. Xu, F. Yang, J. Lin, H. Yang, Y. He. Materials **11**, *10*, 1799 (2018). DOI: 10.3390/ma11101799
[54] S.C. Bhargava, P.K. Iyengar. Phys. Status Solidi B **53**, *1*, 359 (1972). https://doi.org/10.1002/pssb.2220530138.
[55] G.V. Duong, N. Hanh, D.V. Linh, R. Groessinger, P. Weinberger, E. Schafler, M. Zehetbauer. J. Magn. Magn Mater. **311**, *1*, 46 (2007). https://doi.org/10.1016/j.jmmm.2006.11.167.
[56] R.H. Kodama, A.E. Berkowitz, E.J. McNiff, S. Foner. J. Appl. Phys. **81**, *8*, 5552 (1997). DOI: 10.1063/1.364659
[57] A.S. Kamzin, V.G. Semenov, I.A. Al-Omari, V. Narayanaswamy, B. Issa. Phys. Solid State **65**, *8*, 1363 (2023). DOI: 10.21883/PSS.2023.08.56586.122.
[58] A.S. Kamzin, N. Dogan, O.M. Dogan, V.G. Semenov. Phys. Solid State **65**, *8*, 1373 (2023). DOI: 10.21883/PSS.2023.08.56587.127.
[59] K. Haneda, A.H. Morrish. J. Appl. Phys. **63**, *8*, 4258 (1988). DOI: 10.1063/1.340197.
[60] J.M.D. Coey. Phys. Rev. Lett. **27**, *17*, 1140 (1971).
[61] Mossbauer Spectroscopy Applied to Magnetism and Material Science / Eds G.J. Long, F. Grandjean. Plenum Press, N.Y. (1993). 479 p.
[62] A.S. Kamzin, L.P. Ol'khovik, V.L. Rozenbaum. JETP **84**, *4*, 788 (1997).
[63] A.S. Kamzin, L.A. Grigor'ev. Sov. Tech. Phys. Lett. **6**, *6*, 417 (1990).
[64] M.E. Matsnev, V.S. Rusakov. AIP Conf. Proc. **1489**, *1*, 178 (2012).
[65] G.N. Konygin, O.M. Nemtsova, V.E. Porsev. Zhurn. priklad. spektroskopii **86**, *3*, 374 (2019). (in Russian).
[66] S. Mørup. Hyperfine Interactions **90**, 171 (1994). https://doi.org/10.1007/BF02069126
[67] P.V. Hendriksen, C.A. Oxborrow, S. Linderoth, S. Morup, M. Hanson, C. Johansson, F. Bi;ldker, K. Davies, S.W. Charles, S. Wells. Nucl. Instr. Meth. B **76**, 138 (1993).
[68] J. Jing, F. Zhao, X. Yang, U. Gonser. Hyperfine Interactions **54**, 571 (1990).
[69] J. Giri, P. Pradhan, T. Sriharsha, D. Bahadur. AIP J. Appl. Phys. **97**, 10Q916 (2005). https://doi.org/10.1063/1.1855131
[70] R. Hergt, R. Hiergeist, M. Zeisberger, G. Glockl, W. Weitschies, L.P. Ramirez, I. Hilger, W.A. Kaiser. J. Magn. Magn. Mater. **280**, 358 (2004).

Translated by EgoTranslating